Molecular Cell, Volume *81*

Supplemental information

A tamoxifen receptor within

a voltage-gated sodium channel

Altin Sula, David Hollingworth, Leo C.T. Ng, Megan Larmore, Paul G. DeCaen, and B.A. Wallace

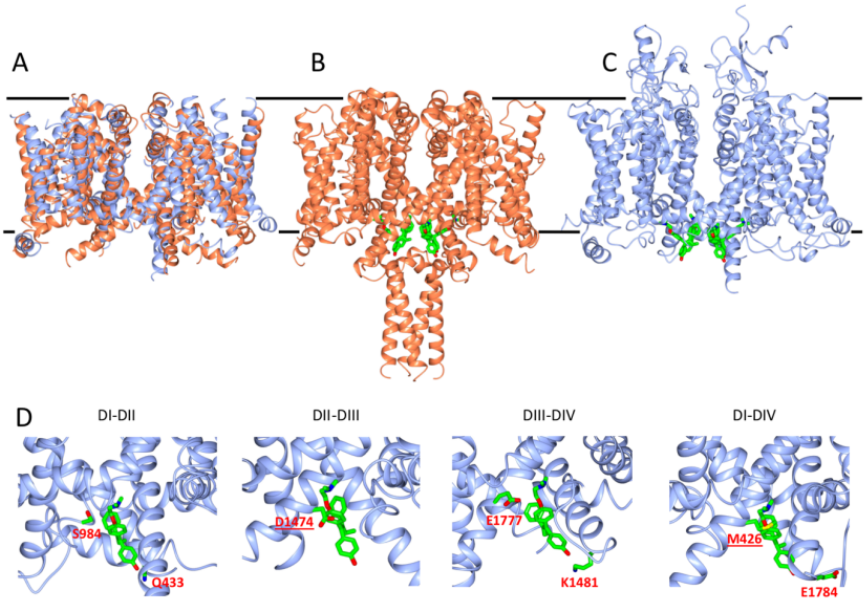

Figure S1. Comparisons of the structures and sequences of NavMs and hNav1.2 (in ribbon representations), Related to Figure 1.

A) Structural alignments of the core residues (not loops or termini) of the NavMs crystal structure (PDB: 5HVX, in orange ribbon depiction) and the hNav1.2 cryo-EM structure (PDB: 6J8E, in blue ribbon depiction), showing the strong similarities of the transmembrane regions (RMSD 3.2Å). The black lines approximate the locations of the membrane surfaces. B) Structure of the full-length NavMs/4-hydroxytamoxifen complex, with 4-hydroxytamoxifen in green stick representation, showing the 4 inner drug binding sites formed between the 4 polypeptide chains in the structure. C) The hNav1.2 structure with 4-hydroxytamoxifen placed into the equivalent site as in NavMs. D) As in C, but showing details of the 4 different potential drug binding sites formed from the 4 different domains (DI-IV) of the hNav1.2 polypeptide chain and the corresponding residues (labelled in red) located at the interfaces between domains (from left to right: DI and DII, DII and DIII, DIII and DIV, DIV and DI). The 4-hydroxytamoxifen does not clash with any protein residues in the DI-DII and DIII-DIV sites, suggesting that the drug could fit at least in two sites in the hNav1.2 structure, but does clash (indicated by the underlined residue labels) with residues in the other two potential sites. E) Sequence alignments of S6 helices of NavMs (Uniprot: A0L556) and human Nav1.2 (hNav1.2) (Uniprot: Q99256) indicating the corresponding residues (in red) in hNav1.2 to those that comprise the tamoxifen binding sites found in NavMs. For each sequence, on the left, the Uniprot codes and the corresponding residue ranges shown are listed, and DI-DIV signify the domain identifiers for hNav1.2. The residues that clash with the drug in the hNav1.2 domain DII-DIII and DIV-DI sites are underlined. [note that one of these potential residues, L991, is not visible in the cryo-EM structure]. The site of the NavMs F208L mutant (designated $NavMs_L$) used in some of these studies is indicated by bold italics. This mutant was used in some of the structures because in half of the $hNa_V1.2$ domains (I and III) it is F and in the other half it is L, and was made so that comparisons could be made to determine if this residue had any effect on the structure (which it didn't, see Figure S6 and Table S1). The sequence alignment was carried out using Clustal Omega (Sievers et al., 2011) and annotated manually.

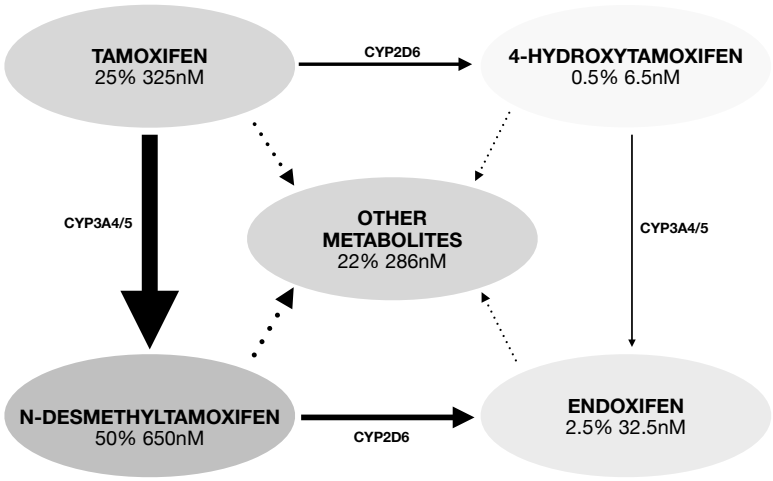

Figure S2. Predominant pathways for cytochrome P450-mediated biotransformation of tamoxifen in human liver, Related to Figure 5.

The enzymes responsible for N-demethylation (CYP3A4/5) and 4-hydroxylation (CYP2D6) produce the metabolites examined in this study, including the most abundant metabolite found in serum, N-desmethyltamoxifen. The proportions and concentrations of tamoxifen and its principle metabolites listed are approximations based on studies of standard 20 mg/day adjuvant tamoxifen therapy, using composite data (based on data from the following references: Errico, 2015; Jordan, 2003; http://clincalc.com/DrugStats/Top3000Drugs.aspx; Shiau et al., 1998; Fraser et al., 2005; Wang et al., 2009; Fraser et al., 2014; Klein et al., 2013; Mürdter et al., 2011; He et al., 2003; Helland et al., 2017; Kisanga et al., 2004; Lien et al., 1991a; Lien et al., 1991b).

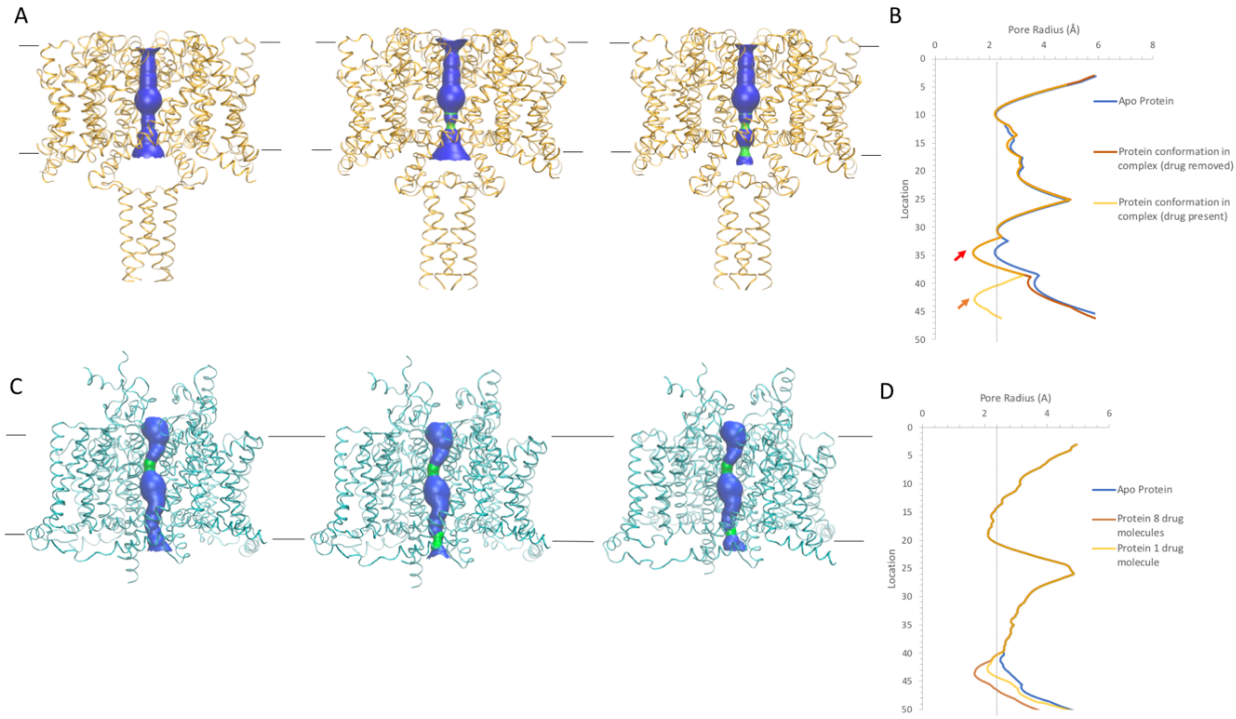

Figure S3. Comparison of the channel dimensions and location of the sodium ion pathway through the transmembrane pore (using the HOLE method (Smart et al., 1993) depicted with VMD software (Humphrey, 1996)), in both the crystal structures of NavMs and the modelled cryo-EM structure (see also Figure S1), both with and without 4-hydroxytamoxifen bound, Related to Figure 2.

A) (Left) The apoNavMs channel. (Middle) The NavMs channel structure in complex with 4-hydroxytamoxifen (but without the drug present) showing the effect of the (small) protein conformational change that occurs upon drug binding. This change involves movement of the I215 side chain, which is not part of in the drug binding site. (Right) The NavMs complex with all eight 4-hydroxytamoxifen molecules included, showing the additional occlusion due to the presence of the drug molecules.

In all three panels, the transmembrane pathway (in the middle of the structure) is depicted in speckled representation. Regions in blue indicate where the pathway is sufficiently wide for sodium ions to pass through, whereas regions in green (in middle and right structures) are where the pore may be too narrow for the passage of sodium ions (Naylor et al., 2016).

B) Accessibility plots for the above structures showing the pore radius of the channel versus position along the pore in the absence (blue) and presence (orange) of 4-hydroxytamoxifen, and of the 4-hydroxytamoxifen complex with the drug (red) removed.

The upper red arrow (at ~ 30 Å) indicates the constriction due to the conformational change in the polypeptide upon binding of the drug, and the lower red arrow (at ~42 Å) indicates the additional constriction due to the presence of the drug. No difference was observed between the structures with all 8 "Inner" and "Outer" sites and those with only the 4 "Inner" better ordered (lower crystal structure B factors) sites occupied.

C) (Left) The apo-h$Na_V1.2$ cryoEM structure, showing the constriction in the selectivity filter region (green) and the wider pathway elsewhere in the transmembrane pathway. (Middle) The additional constriction (green, near the bottom) is due to the inclusion of four 4-hydroxytamoxifen molecules in the equivalent positions as found in NavMs. (Right) As in B, but with only one drug molecule added at a site equivalent to an "Inner" site in NavMs.

D) Plot (as in B) showing a similar narrowing in the selectivity filter region (~20 Å) as seen in NavMs, and an additional constriction (~43 Å) near the pore exit near the intracellular surface in the presence of one or more drug molecules. No difference was observed between the structures with all 8 sites and those with only the 4 inner sites occupied.

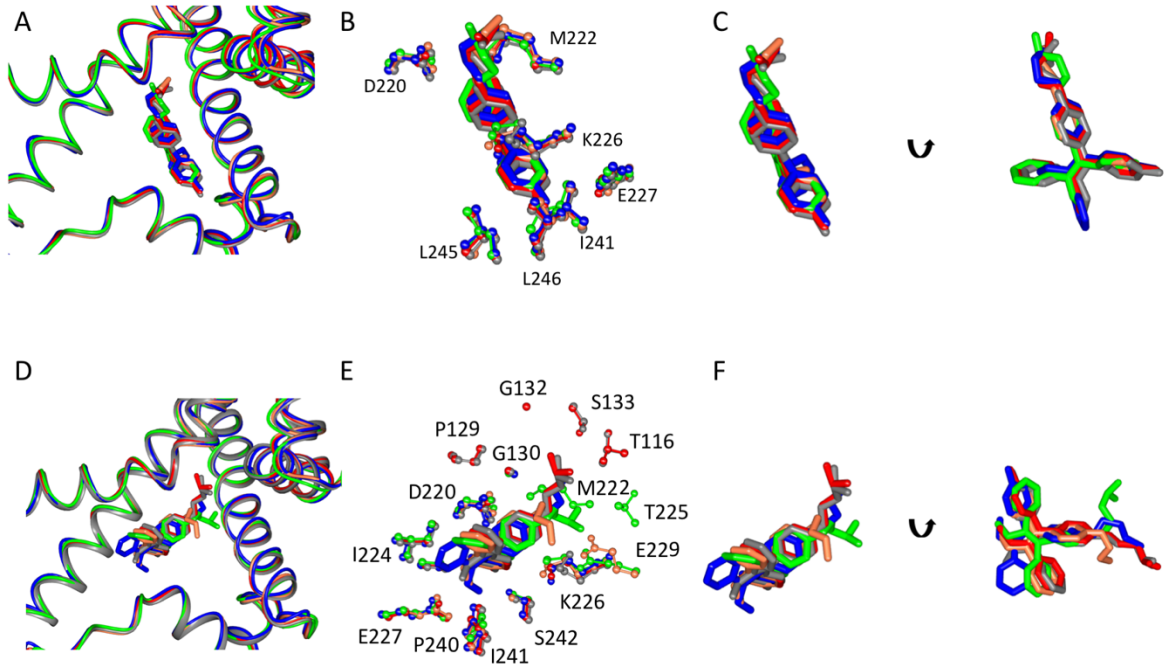

Figure S4. Comparisons of Inner and Outer sites in the 4 different NavMs$_L$ drug complexes of tamoxifen (green), 4-hydroxytamoxifen (red), N-desmethyltamoxifen (coral), and endoxifen (blue) and NavMs (wild type) in complex with 4-hydroxytamoxifen (grey), Related to Figure 3.

A-C) Comparisons of the "Inner" binding sites: A) Aligned crystal structure of five complexes (in ribbon depiction for 2 of the polypeptide chains, which are coloured as described in the title of this figure. The drugs in the inner site shown in stick depiction (the RMSD between them is 0.3-0.6A). B) An expanded view of the inner site showing the drugs and their binding residues (in corresponding colours) that lie within a 4 Å distance for all five structures. All of the binding residues are the same in all 5 structures.

Panel C shows two views of just the "Inner" ligand binding sites. The arrow indicates how the left and right views are rotated in order to give two views of each site. E227 and D220 are the residues that were modified in the electrophysiology studies.

D- F) Comparisons of the "Outer" binding sites: A) Aligned crystal structure of the five complexes (as in (panel A). The drugs are shown in stick depiction (the RMSD between them is 1.6-1.9 Å). E) As in B) for the outer site drugs but showing their binding residues (within a 4 Å distance of the drug atoms) for all five structures coloured in the corresponding colours. As the drugs adopt many different conformations within the Outer site, many more of the protein residues fall in this region.

C) Two views of the ligand in the "Outer" ligand binding sites. The arrow indicates how the left and right views are rotated in order to give two views of each site.

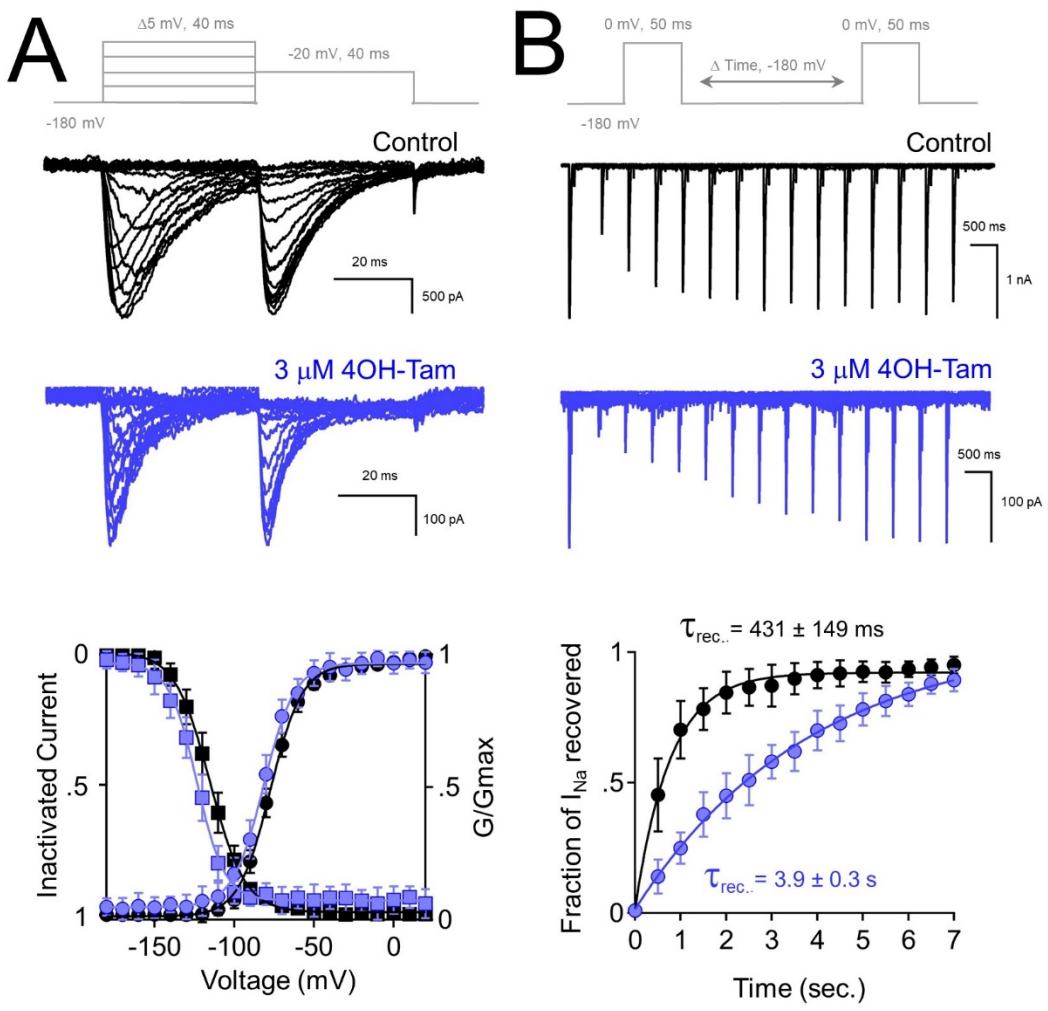

Figure S5. 4-Hydroxytamoxifen impairs NavMs recovery from inactivation but does not its voltage dependence, Related to Figure 6.

Voltage protocols are shown in grey above each panel. A) The impact of tamoxifen treatment on NavMs voltage dependence. *Top*, Exemplar I_{Na} currents recorded in control and 4-hydroxytamoxifen conditions. *Middle*, sodium currents were activated by 40 ms test pulse of increasing potential followed by a test pulse to −20 mV. *Bottom*, resulting conductance-voltage and inactivation-voltage relationships were measured by plotting the average conductance and reduction of test I_{Na}, respectively, as a function of prepulse potential. Both relationships were fit to a Boltzmann equation. The voltage dependences of inactivation in the control and after drug treatment were equal to -116 ± 6 mV and -122 ± 8 mV, respectively, and were not statically different ($P = 0.2$), based on results from a two-tailed Student's t-test (n = 5 cells, Error = S.D.).

B) Current records testing the recovery from inactivation ($\tau_{rec.}$) by the NavMs channel before and after 4-hydroxytamoxifen treatment. *Top*, exemplar sodium currents inactivated by 50 ms pre-pulse to -20 mV and an identical test pulse separated by increasing recovery times. *Bottom*, The ratio of test pulse and pre-pulse current is plotted as a function of recovery time and fit to single exponential equation to establish the recovery time constant (n = 4-6 cells, Error = S.D.).

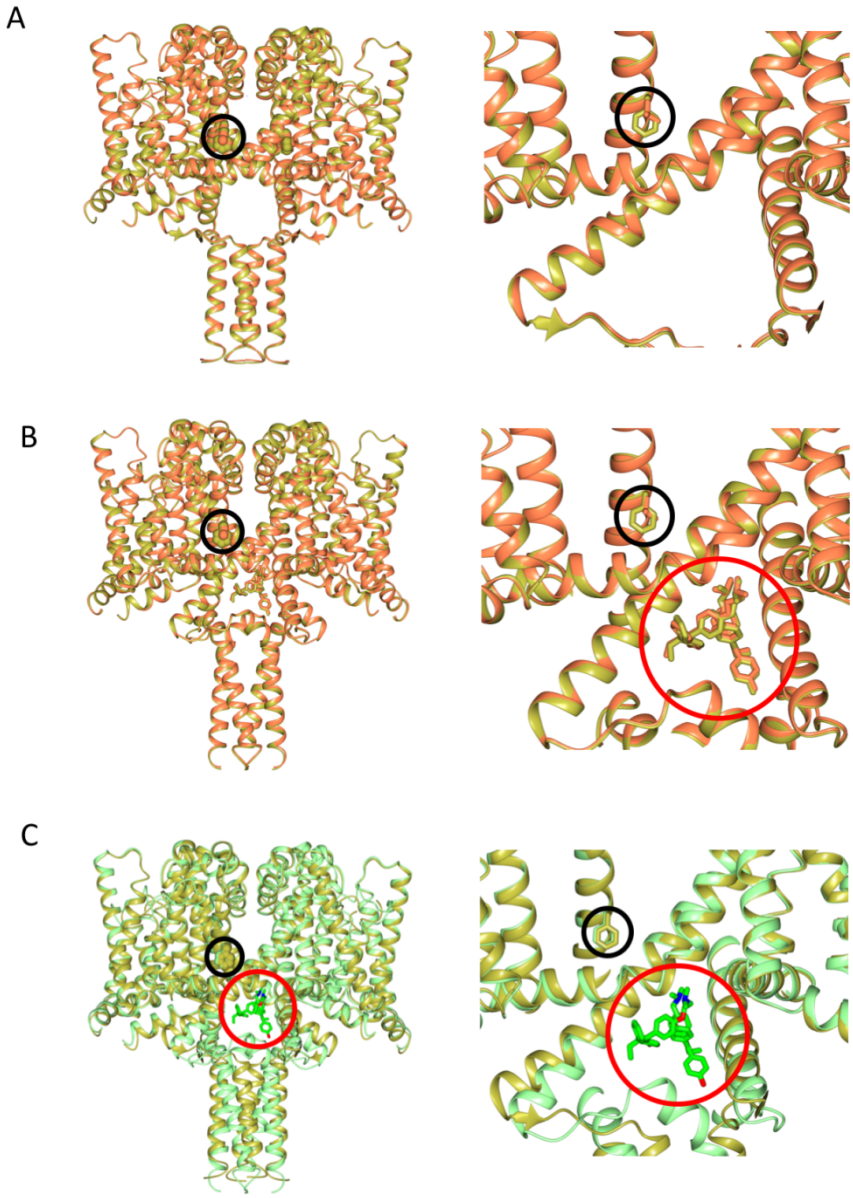

Figure S6. Comparisons of wild type NavMs (PDB: 5HVX) with NavMs$_L$ (PDB: 6SXS) structures, and of apoNavMs with the NavMs/4-hydroxytamoxifen complex (PDB: 6SXG) structure, Related to Figure 1 and STAR Methods.

A) (Left) Overlay of the apo structures of NavMs (gold) and NavMs$_L$ (coral) showing their overall structures are nearly identical (C_a RMSD = 0.36 Å). (Right) Detailed view showing the close similarities of the structures in the region of the mutated residue (F208L, which is circled in black in both panels).

B) As in A) except comparing the 4-hydroxytamoxifen complexes of NavMs and NavMs$_L$ (C_a RMSD = 0.29 Å).

C) (Left) Overlay of apoNavMs (gold) and its 4-hydroxytamoxifen complex (green) (C_α overall RMSD = 1.3 Å). (Right) Detailed view of the binding site region. The black circle indicates the position of the F208 residue, showing that this region of the structure is the same in the apo- and complex structures. The red circle indicates the location of the two drug molecules (in stick depiction) molecule in the structure of the complex.

Table S1. Crystal Structure Data Collection and Refinement Statistics, related to Figure 1.

Data collection Samples (and PDB codes)	**$NavMs_L$ (6SX5)**	**$NavMs_L$/ Tamoxifen (6SXF)**	**NavMs/ 4-hydroxy-tamoxifen (6SXG)**	**$NavMs_L$/ 4-hydroxy-tamoxifen (6SXC)**	**$NavMs_L$/ Endoxifen (6SXE)**	**$NavMs_L$/ N-desmethyl-tamoxifen (6Z8C)**	**$NavMs_{L/}$/ DMSO (6SX7)**
Wavelength (Å)	0.96881	0.96881	0.97970	0.97620	0.97966	0.96864	0.97624
Space group	I422	$P42_12$	I422	I422	I422	I422	I422
Unit-cell parameters							
a, b, c (Å)	109.13 109.13 209.03	107.99 107.99 212.17	108.87 108.95 211.29	109.12 109.12 210.60	109.58 109.58 209.71	109.22 109.22 211.16	109.00 109.00 208.83
α, β, γ (°)	90, 90, 90	90, 90, 90	90, 90, 90	90, 90, 90	90, 90, 90	90, 90, 90	90, 90, 90
Resolution range (Å)	43.27-2.2 (2.27-2.20)	76.36-2.84 (2.91-2.84)	48.4-2.4 (2.49-2.40)	48.44-2.5 (2.6-2.50)	97.53-2.6 (2.72-2.60)	48.51-3.2 (2.42-3.20)	62.01-2.5 (2.6-2.50)
Total number of observations	617668 (43897)	468596 (34685)	406860 (43496)	484502 (55271)	263748 (33637)	155501 (28406)	365409 (39940)
Total number unique	32440 (2774)	30492 (2195)	25305 (2619)	22430 (2478)	20152 (2435)	10937 (1934)	22217 (2459)
Completeness	100.0 (100)	100.0 (100)	100.0 (100)	100.0 (99.7)	99.1 (100)	100.0 (100)	100.0 (100)
Multiplicity	19.0 (15.8)	15.4 (15.8)	16.1 (16.6)	21.6 (22.3)	13.1 (13.8)	14.2 (14.7)	16.4 (16.2)
$\langle I/\sigma(I)\rangle$	14.0 (4.5)	6.3 (1.2)	20.4 (3.8)	19.5 (2.5)	14.6 (1.6)	6.6 (1.4)	15.1 (2.8)
CC(1/2)	0.99 (0.97)	0.98 (0.87)	0.99 (0.97)	1 (0.96)	0.99 (0.83)	0.99 (0.81)	0.99 (0.96)
R_{merge}	0.12 (0.578)	0.26 (2.4)	0.10 (1.80)	0.1 (1.2)	0.29 (3.6)	0.27 (1.77)	0.15 (2.14)
R_{pim}	0.039 (0.209)	0.072 (0.62)	0.043 (0.72)	0.023 (0.268)	0.045 (0.095)	0.076 (0.49)	0.054 (0.788)
Solvent content (%)	0.728	0.742	0.742	0.742	0.742	0.742	0.742
Molecule per ASU	1	2	1	1	1	1	1
Wilson B factor ($Å^2$)	40.88	71.0	58.7	64.72	74.3	77.5	58.8
Refinement							
Resolution Range (Å)	28.8-2.20	35.91-2.84	26.57-2.4	26.4-2.5	52.54-2.6	48.5-3.2	27.25-2.5
R_{work}	0.22 (0.20)	0.23(0.256)	0.221(0.19)	0.23(23.48)	0.24 (19.21)	0.25 (25.48)	0.23 (21.92)
R_{free}	0.24 (0.21)	0.26 (0.303)	0.261 (0.20)	0.25 (27.96)	0.28 (21.00)	0.27 (29.96)	0.25 (23.77)
Reflection, working	32421	30416	25285	22408	20151	11540	22192
Reflection, free	1619	1520	1264	1148	1007	577	1141
All atoms Average B factor	77.0	91.96	89.57	90.0	108.0	85.0	88.1
'Inner' Drug B factor	=	110	86	96	109	104	=
'Outer' Drug B factor	=	153	120	144	218	169	=
Rmsd bond angle	0.95	1.05	0.98	1.04	1.04	0.89	0.99
Rmsd bond length (Å)	0.010	0.007	0.08	0.009	0.010	0.008	0.011
Ramachandran Analysis							
Preferred region (%)	96.6	98.0	97.8	96.3	97.0	96.6	98.8
Allowed region (%)	3.0	2.0	1.8	3.0	2.6	3.0	1.2
Outliers (%)	0.4	0.0	0.4	0.7	0.4	0.4	0.0

$R_{merge} = \Sigma\ (I - \langle I\rangle) / \Sigma\langle I\rangle$

$R_{work} = \Sigma\ (|F_{obs}| - |F_{calc}|)/ \Sigma|F_{obs}|$ for 95% of data. Rfree is the same equation for 5% of the data excluded from refinement.